ADVANCED FUNCTIONAL MATERIALS
www.afm-journal.de

On-Chip Fabrication of Paclitaxel-Loaded Chitosan Nanoparticles for Cancer Therapeutics

Fatemeh Sadat Majedi, Mohammad Mahdi Hasani-Sadrabadi, Jules John VanDersarl, Nassir Mokarram, Shahirar Hojjati-Emami, Erfan Dashtimoghadam, Shahin Bonakdar, Mohammad Ali Shokrgozar, Arnaud Bertsch, and Philippe Renaud**

The use of solvent-free microfluidics to fine-tune the physical and chemical properties of chitosan nanoparticles for drug delivery is demonstrated. Nanoparticle self-assembly is driven by pH changes in a water environment, which increases biocompatibility by avoiding organic solvent contamination common with traditional techniques. Controlling the time of mixing (2.5–75 ms) during nanoparticle self-assembly enables us to adjust nanoparticle size and surface potential in order to maximize cellular uptake, which in turn dramatically increases drug effectiveness. The compact nanostructure of these nanoparticles preserves drug potency better than previous nanoparticles, and is more stable during long-term circulation at physiological pH. However, when the nanoparticles encounter a tumor cell and the associated drop in pH, the drug contents are released. Moreover, the loading efficiency of hydrophobic drugs into the nanoparticles increases significantly from previous work to over 95%. The microfluidic techniques used here have applications not just for drug-carrying nanoparticle fabrication, but also for the better control of virtually any self-assembly process.

1. Introduction

The search for effective cancer treatments has long been the focus of numerous scientists,[1] and increasing worldwide cancer incidence rates have only intensified the search for efficient therapeutic techniques.[2] A major component of current research is not concerned with developing stronger drugs, but rather minimizing the impact anti-cancer drugs have on normal cells, with tumor seeking "smart drugs" as the ultimate goal. In an effort to reach this goal, targeted drug delivery systems (DDS) based on polymeric nanoparticles have emerged as a promising strategy.[3,4] Chitosan, a polysaccharide found in the protective shells of shrimp and other crustaceans, is a promising building block for constructing drug delivery nanoparticles, as it is inexpensive, has easily modifiable functional groups,[5] and the size and shape of chitosan nanoparticles can be precisely controlled.[6,7] Although the hydrophilic nature of chitosan does not normally allow for the loading of most hydrophobic anticancer drugs, chitosan modification via N-palmitoyl groups has been demonstrated to enable such loading.[8–10] This modification also allows for nanoparticles to be packed via ionic gelation[11,12] rather than chemical cross-linking,[12] the standard technique for chitosan nanoparticle synthesis. Avoiding chemical crosslinking is desirable, as there are frequently problems related to the removal of chemical crosslinking agents from assembled nanoparticles. Unfortunately, nanoparticle self-assembly with simple bulk mixing produces extremely polydisperse chitosan nanoparticles, which in turn exhibit a wide range of mechanical and chemical properties. However, we can create small and monodisperse nanoparticles with microfluidic synthesis,[10] by

F. S. Majedi, M. M. Hasani-Sadrabadi, Dr. J. J. VanDersarl, Dr. A. Bertsch, Prof. P. Renaud
Laboratoire de Microsystemes (LMIS4)
Institute of Microengineering
École Polytechnique Fédérale de Lausanne (EPFL)
CH-1015, Lausanne, Switzerland
E-mail: jules.vandersarl@epfl.ch; philippe.renaud@epfl.ch
N. Mokarram
School of Materials Science and Engineering
Georgia Institute of Technology and Emory University
Atlanta, GA, 30332, USA
F. S. Majedi, M. M. Hasani-Sadrabadi, Dr. S. Hojjati-Emami
Department of Biomedical Engineering
Amirkabir University of Technology
Tehran, Iran
M. M. Hasani-Sadrabadi, Dr. E. Dashtimoghadam
Department of Polymer Engineering
and Color Technology
Amirkabir University of Technology
Tehran, Iran
Dr. S. Bonakdar, Prof. M. A. Shokrgozar
National Cell Bank of Iran
Pasteur Institute of Iran, Tehran, Iran

DOI: 10.1002/adfm.201301628

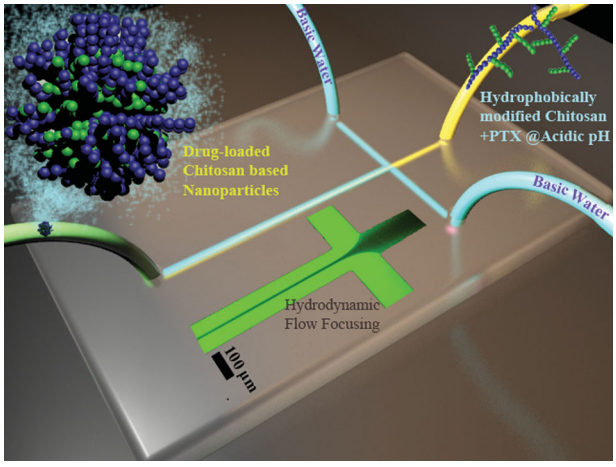

Scheme 1. (a) Schematic representation of a T-shaped microfluidic device, which is used to hydrodynamically flow focus HMCS using a sheath flow of water at basic pH. Inset is a fluorescence image of Rhodamine B hydrodynamically focused with Fluorescein sodium streams (scale bar 100 µm). (b) Schematic representation of HMCS nanoparticle circulation and localized drug release.

creating a narrowly defined mixing regime via hydrodynamic flow focusing.[13,14] This well-controlled mixing regime can be precisely adjusted with the microfluidic platform (primarily through flow ratio and velocity) and is crucial in creating monodisperse nanoparticles with tunable properties, including drug encapsulation efficiency and release rate.

2. Results and Discussion

We developed a T-shape microfluidic device to create hydrodynamically focused flow. As shown in **Scheme 1**, the microfluidic device consists of two inlets for water at a basic pH (pH 9.0), one for the HMCS (high molecular weight chitosan supplement) solution at an acidic pH (pH 4.5), and one outlet for the fabricated nanoparticles. Stability of the flow at different flow rates was verified using fluorescence microscopy, with Rhodamine B and fluorescein sodium mixed in the core flow and sheath flow, respectively (Inset of Scheme (1). A critical parameter in determining nanoparticle size is the mixing time, τ_{mix}, which can be estimated from Equation (1), [15]

$$\tau_{mix} \sim \frac{w_f^2}{4D} \approx \frac{w^2}{9D} \frac{1}{\left(1 + {}^1/_R\right)^2} \quad (1)$$

where w is the channel width (150 µm), D is the diffusion constant (10^{-9} $m^2.s^{-1}$) and R is the ratio of the polymeric stream and basic water flow rates (R = 0.03–0.2). w_f can be estimated as the width of the focused chitosan stream when R < 1. Equation (1) estimates our microfluidic platform can achieve any mixing time between 2.5 and 75 ms.

In acidic solutions HMCS acts as a polyelectrolyte, due to protonated amine groups ($-NH_3^+$) and grafted hydrophobic side chains. The solution pH controls the balance between electrostatic repulsion and hydrophobic attraction forces. An increase in pH, which occurs in the microfluidic device as a result of diffusion between the lateral and central streams, drives the particles to self-assemble. This phenomenon occurs due to the simultaneous deprotonaion of HMCS chains, which reduces electrostatic repulsion, and amine group deprotonation, which are then free to form hydrogen bonds with the hydroxyl groups.[16] The hydrophobic moieties of the polymers result in a strong driving force towards self-aggregation. This process is regulated on our microfluidic device through precise control of the time of mixing (τ_{mix}, Equation (1) between the streams, which allows us to form stable HMCS nanoparticles at a physiological pH.

The effect of the flow ratio on the size of formed nanoparticles is shown in **Figure 1**a. HMCS with three different degrees of substitution, 8.6 ± 0.3 (DS I), 14.5 ± 0.3 (DS II), and 18.2 ± 0.3 (DS III) mol% (based on the ninhydrin assay,[17,18] were used. The hydrodynamic diameter of the self-assembled nanoparticles is controlled by changing the flow ratios and the degree of HMCS chain hydrophobicity (Figure 1).

The mixing time used for self-assembly is kept in the millisecond range *via* changing the flow ratio of HMCS to water streams from 0.03 to 0.2. Results indicate that time of mixing, τ_{mix}, varies from approximately 2.5 to 75 ms (Equation (1). If $\tau_{mix} < \tau_{agg}$ (the time of aggregation) we produce kinetically locked nanoparticles, which prevents their further growth, and keeps their final size smaller and more monodisperse than any bulk method.[10,19] Previously we have reported a 20–30 ms time as the aggregation time, τ_{agg}, for chitosan based nanoparticles.[19]

By controlling the flow ratio, we can create nanoparticles at a specific size, as it determines the mixing time during particle self-assembly. The diameter of the nanoparticles increases with an increase in flow ratio. At a specific flow ratio, particle size decreases with increasing hydrophobic group concentration (DS I > DS II > DS III). These observations are consistent with previously reported results, and can be attributed to the increase in hydrophobicity between the conjugated C_{12} groups.[9] Based on our previous work, for chitosan based systems a flow ratio of about 0.12 is the transition point between the rapid mixing ($\tau_{mix} < \tau_{agg}$) and slow mixing ($\tau_{mix} > \tau_{agg}$) regimes.[10,19] Other researchers have found sharper regime transitions during solvent exchange induced self-assembly, but these occurred under rapid micromixing of supersaturated block copolymers.[20]

Nanoparticles synthesized with microfluidics were consistently smaller than those prepared through bulk mixing, across all flow ratios and hydrophobic levels. Moreover, the polydispersity index (PI) for the microfluidic nanoparticles was found to be remarkably lower (PI < 0.2) than bulk synthesized particles (PI > 0.6) (Table S1). Turbulent mixing is thought to be the main reason, as it results in a broad distribution of residence times in bulk mixing methods.[12] However, our microfluidic method for HMCS nanoparticle assembly is reproducible and independent of user talent, due to the well-controlled hydrodynamically focused area. Under this condition, deprotonation of HMCS amine groups occurs before polymer aggregation. As a result, nanoparticle assembly occurs at a pH close to physiological conditions. A similar mechanism has been suggested to drive microfluidic nanoprecipitation.[15,21,22] However, during bulk mixing nanoparticle assembly occurs faster than the pH change, which results in an increase in structural heterogeneity. Our microfluidic nanoparticle assembly occurs at the final pH.

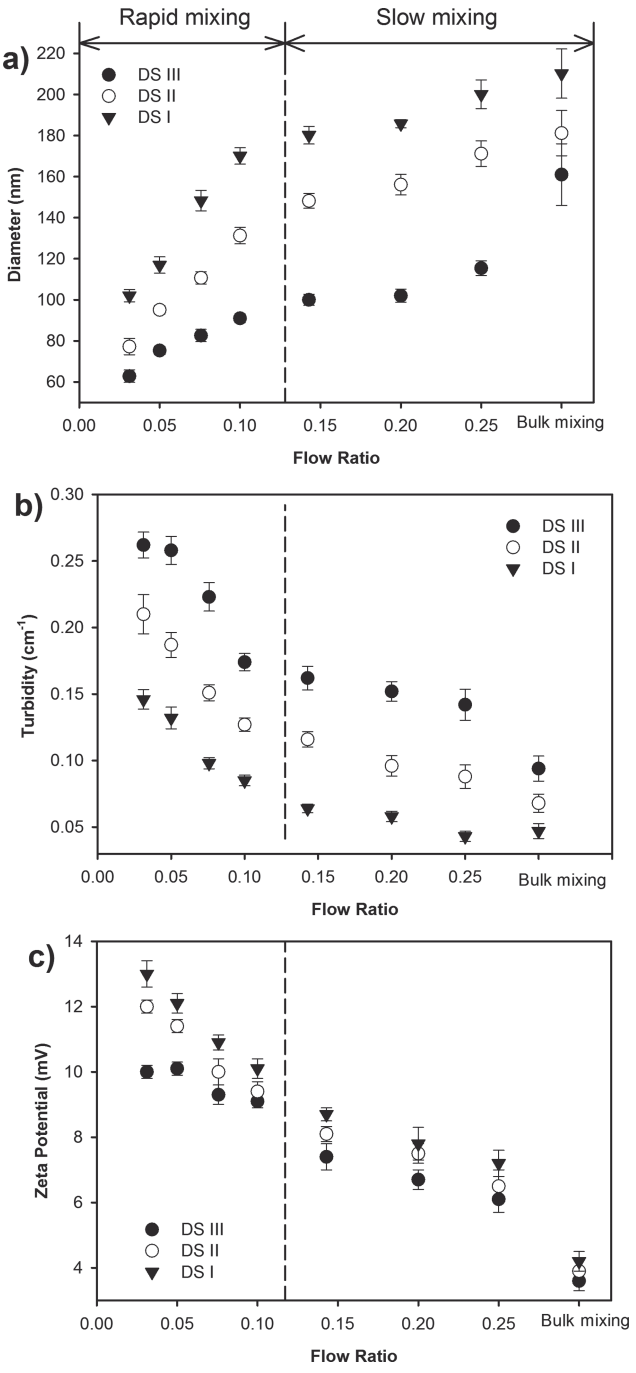

Figure 1. Effect of flow ratio on (a) diameter (based on DLS results) (b) turbidity, and (c) zeta potential of synthesized nanoparticles without paclitaxel (PTX) drug.

Having a narrow particle size distribution requires fast nucleation followed by the growth of nanoparticles in the absence of further nucleation. Moreover, turbidity values of nanoparticles, as an indicator of their compactness,[23,24] are shown in Figure 1b. Less compact nanoparticles occur during bulk mixing, which results in turbidity lower than all particles derived from our microfluidic system. These results confirm the ability of our microfluidic synthesizing approach to produce more compact nanoparticles, especially at higher hydrophobicity levels and lower times of mixing, than would be possible using standard bulk mixing.

The microfluidically synthesized nanoparticles were also found to be more charged compared to previously reported results for chitosan nanoparticles formed with bulk mixing.[8,10] According to zeta potential measurements (Zetasizer 3000HS), the surface charge of HMCS nanoparticles produced at flow ratio 0.1 in physiological pH are +10 ± 0.2 mV (DS III), +12 ± 0.2 mV (DS II), and +13 ± 0.4 mV (DS I), which are about three times higher than the surface charges of bulk synthesized nanoparticles, which are +3.6 ± 0.3 mV (DS III), +3.9 ± 0.4 mV (DS II), and +4.2 ± 0.3 mV (DS I) (Figure 1c). This phenomenon is a consequence of rapid mixing during microfluidic nanoparticle formation, which allows the polymer hydrophobic groups to perfectly bury their heads, thus leaving more amine groups exposed on the nanoparticle surface. Likely due to the fact that cell surfaces are mostly anionic, cationic particles has been reported to be endocytosed at increased rates.[25] Due to the exposed amine groups on our microfluidic nanoparticles, and thus their cationic nature, we have observed increased cellular uptake of our nanoparticles prepared with microfluidics. The ideal nanoparticle surface charge for endocytosis enhancement is reported to be between10–15 mV,[26] which is about the charge on our nanoparticles (Figure 1c).

HMCS nanoparticle morphology trends found through dynamic light scattering analysis were confirmed with transmission electron microscopy (TEM) and atomic force microscopy (AFM). As shown in Figure 1a, the on-chip synthesized nanoparticles are smaller than bulk synthesized particles, with particle size further decreased at higher flow ratios. Nanoparticles prepared with the microfluidic platform also have a much narrower size distribution than those prepared through bulk mixing (Table S1), with the most uniform particles resulting from the shortest time of mixing. As seen in **Figure 2**, TEM images show nanoparticle sizes to be in good agreement with the dynamic light scattering results exhibited in Figure 1a. As shown in Figure 1b, the on-chip synthesized nanoparticles are more compact than bulk synthesized nanoparticles, which results in higher turbidity. These nanoparticle compactness trends are confirmed through TEM analysis (Figure 2).

AFM images of HMCS nanoparticles synthesized through bulk mixing and microfluidics at a flow ratio of 0.03 are shown in Supporting Information Figure S1. These results are in agreement with TEM and DLS results.

Particle stability was also investigated at 25 °C for one month (Supporting Information Figure S2). Particles formed at low flow ratios (rapid mixing) are more stable than those formed at higher flow ratios and during bulk mixing. This can be attributed to the more efficient burying of HMCS hydrophobic side groups during nanoparticle formation in the rapid mixing regime, which is confirmed by Zeta potential results.

The pH sensitivity of these nanoparticles relates to the density of ionizable groups in the HMCS structures. Behavior of the particles was studied at three different pH levels, 7.4, 6.5, and 5.5, in order to mimic the environments of blood plasma, a tumor, and endosomes,[27] respectively. As the pH lowers, the nanoparticles start to swell due to the protonation of more amine groups, which generates additional charge repulsion.

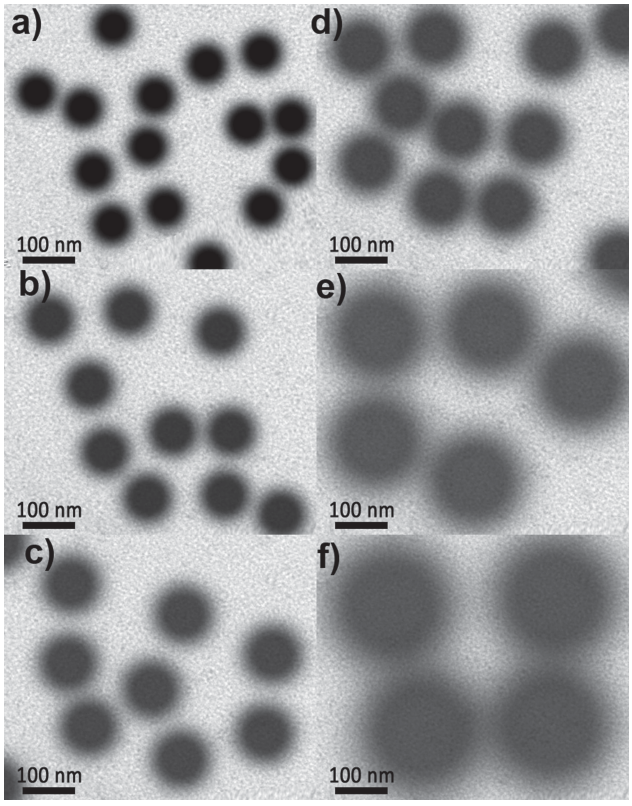

Figure 2. TEM images of HMCS nanoparticles synthesized at flow ratio 0.03 using HMCS with a degree of substitution of (a) DSIII, (b) DSII, and (c) DSI in comparison with bulk synthesized nanoparticles with a degree of substitution of (d) DSIII, (e) DSII, and (f) DSI.

From this, we can tune drug release in response to pH changes. The pH sensitivity of microfluidic synthesized nanoparticles is lower than that of bulk synthesized ones. This can be attributed to the more compact nanostructure of microfluidic synthesized nanoparticles (Supporting Information Figure S3).

To date, there has not been a detailed investigation on the influence of the size and surface charge of nanoparticles on their biodistribution, pharmacokinetics, tumor penetration and cellular uptake.[28] However, as previously mentioned, the surface charge as well as the size of our NPs is in a desirable range for cellular endocytosis. Surface charge is also known to affect important properties such as nanoparticle blood circulation time, which may push the ideal zeta potential for certain applications outside the 10–15 mV range. This uncertainty only emphasizes the importance of a flexible platform that can produce nanoparticles with properties tunable across a wide parameter space.

To evaluate cellular internalization of our NPs, MCF-7 cells were cultured for 2 h with FITC labeled NPs (f-HMCS NPs). After culture, the cells were rinsed with EDTA (pH 5.0) to remove surface bound NPs,[29] and then quantified for fluorescence intensity, and therefore degree of NP uptake, with flow cytometry. The NPs prepared with microfluidics were theorized to be internalized at a higher rate than the NPs prepared via bulk mixing due to their higher surface charge. Indeed, the fluorescence intensity of the cells cultured with microfluidic

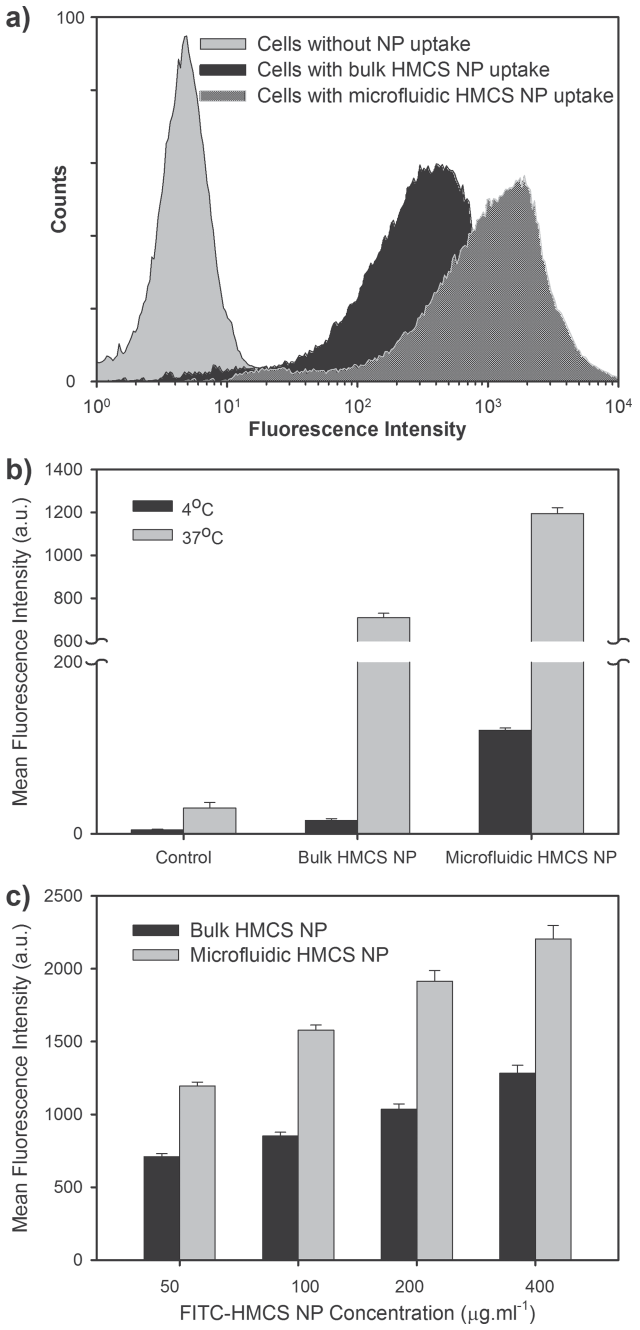

Figure 3. (a) Cellular uptake of HMCS NPs labeled with FITC and measured by flow cytometry. (b) Temperature-dependent cellular uptake based on median fluorescent intensity at 4 °C (black) and 37 °C (grey). (c) Cellular uptake as a function of NPs concentration for bulk (black) and microfluidic (grey) based f-HMCS NPs. Values indicate mean ± one standard deviation from three independent measurements performed in triplicate.

f-HMCS NPs was 1.7-fold higher than that of cells cultured with bulk f-HMCS NPs ($P < 0.01$) (**Figure 3**). We also performed experiments where the cells and NPs were incubated at 4 °C, were endocytosis is strongly inhibited.[30] Lowering the incubation temperature from 37 °C to 4 °C considerably reduced the amount of fluorescence for both types of NPs (Figure 3b),

indicating endocytosis is the dominant mechanism for nanoparticle uptake. Still, the fluorescence intensity of microfluidic NP cells was much brighter than bulk mixing NP cells (Figure 3b).

The amphiphilic nature of HMCS allows us encapsulate both hydrophilic and hydrophobic agents. Here, the ability of our microfluidic platform to encapsulate a well-known hydrophobic anticancer drug, paclitaxel (PTX), is evaluated. An acidic condition during the injection of HMCS/PTX prevents PTX epimerization and prolongs its activity.[31] PTX loaded nanoparticles (Supporting Information Figure S4) are consistently larger than their unloaded counterparts (Figure 1a). PTX increases the final size of the particles between 10-20% for the highest degree of substitution (DS III) polymers and 28–38% for lower DS (DS II and DS I). Despite the size increase, HMCS nanoparticles remain in the acceptable size range for passive targeted drug delivery, which causes them to enhance their penetration and accumulation in tumor sites. [2,4,5]

PTX encapsulation efficiency, the fraction of available PTX incorporated into the HMCS nanoparticles, was investigated and summarized in **Figure 4**. At constant flow ratios, encapsulation efficiency increases at higher HMCS DS due to the hydrophobic nature of PTX (Figure 4a). Moreover, at shorter mixing times, more hydrophobic moieties are involved and interact with PTX molecules during the formation of nanoparticles, resulting in higher encapsulation efficiencies. This trend begins with the transition from the rapid mixing to the slow mixing regimes.

Encapsulation efficiency was also affected by the initial PTX concentration. Figure 4b summarizes PTX loading efficiency at 5, 10, 15, and 20 wt% at various nanoparticle assembly rates. As shown, particle loading content is significantly affected by the mixing regime (rapid or slow). Our polymeric nanoparticles can reach loading efficiencies of 95% or higher through the application of microfluidic assembly. High loading efficiencies are desirable as they help reduce the needed drug dosage, and increase therapeutic efficiency.

The in vitro release profiles of the microfluidic synthesized PTX-loaded nanoparticles, with DSIII HMCS, were compared with bulk-synthesized nanoparticles in PBS (phosphate buffer solution) at pH 7.4 and 5.5 over two weeks (**Figure 5**).

The required times to release half of the loaded drugs (t_{50}) from the nanoparticles is shown in Figure 5c. Normally, larger NPs with the same compactness should show slower release profiles, due to longer diffusion distances for drugs to leave the nanoparticle core and the lower surface to volume ratios. But since the method of synthesis affects compactness too, it seems that the release behavior of the microfluidic synthesized nanoparticle has a direct relationship between release rate and particle size due to the decrease in compactness which occurs as we go from the smallest flow ratio to bulk mixing, except for DS III-FL 0.031, which is formed at the rapid mixing regime (τ_{agg} = 2.5) ms, where the higher surface to volume ratio of the smallest particles makes them release their contents faster.

Therefore, for nanoparticles which are formed in the rapid mixing regime (FL.031 and FL.075).[32] a reduction in pH significantly increases the initial (<24 h) release rate (Figure 5b,d, and Figure S5) due to the pH sensitivity and resultant swelling of the nanoparticles as described previously (Supporting Information Figure S3). Furthermore, all nanoparticles fully release

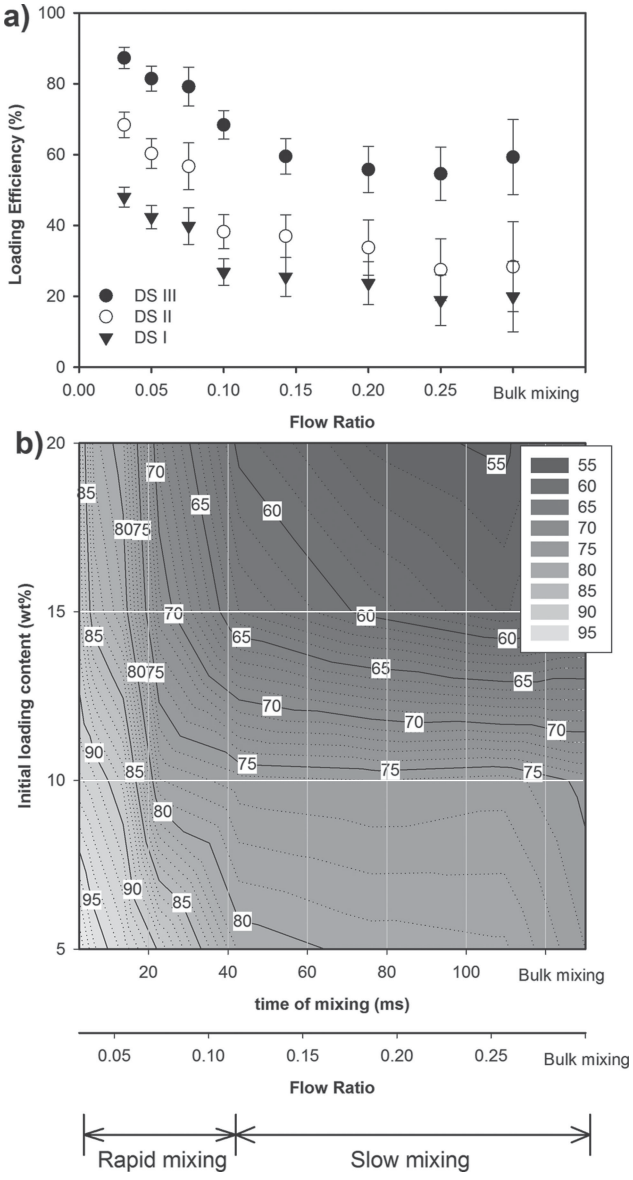

Figure 4. (a) The change in paclitaxel (PTX) loading efficiency as a function of degree of substitution (DS) for nanoparticles formed at various flow ratios or with bulk mixing. (b) A contour plot for PTX loading efficiency (DSIII), as a function of time of mixing and initial loading PTX concentration. (Mean ± SD, n = 5 independent experiments).

their PTX contents at pH 5.5, whereas microfluidic nanoparticles were able to keep their PTX cargo for much longer at pH7.4 (Figure 5a,b).

The tuning capability of the nanoparticle drug release behavior, and the diffusion coefficient of PTX molecules within the nanoparticles, was also investigated through the fraction of released drug and the square root of time according to Equation (2),[33]

$$\frac{M_t}{M_\infty} = 6\left(\frac{Dt}{\pi R^2}\right)^{1/2} \quad (2)$$

where M_t/M_∞ represents the fraction of released drug at time t, D is the diffusion coefficient of the drug molecules and R is

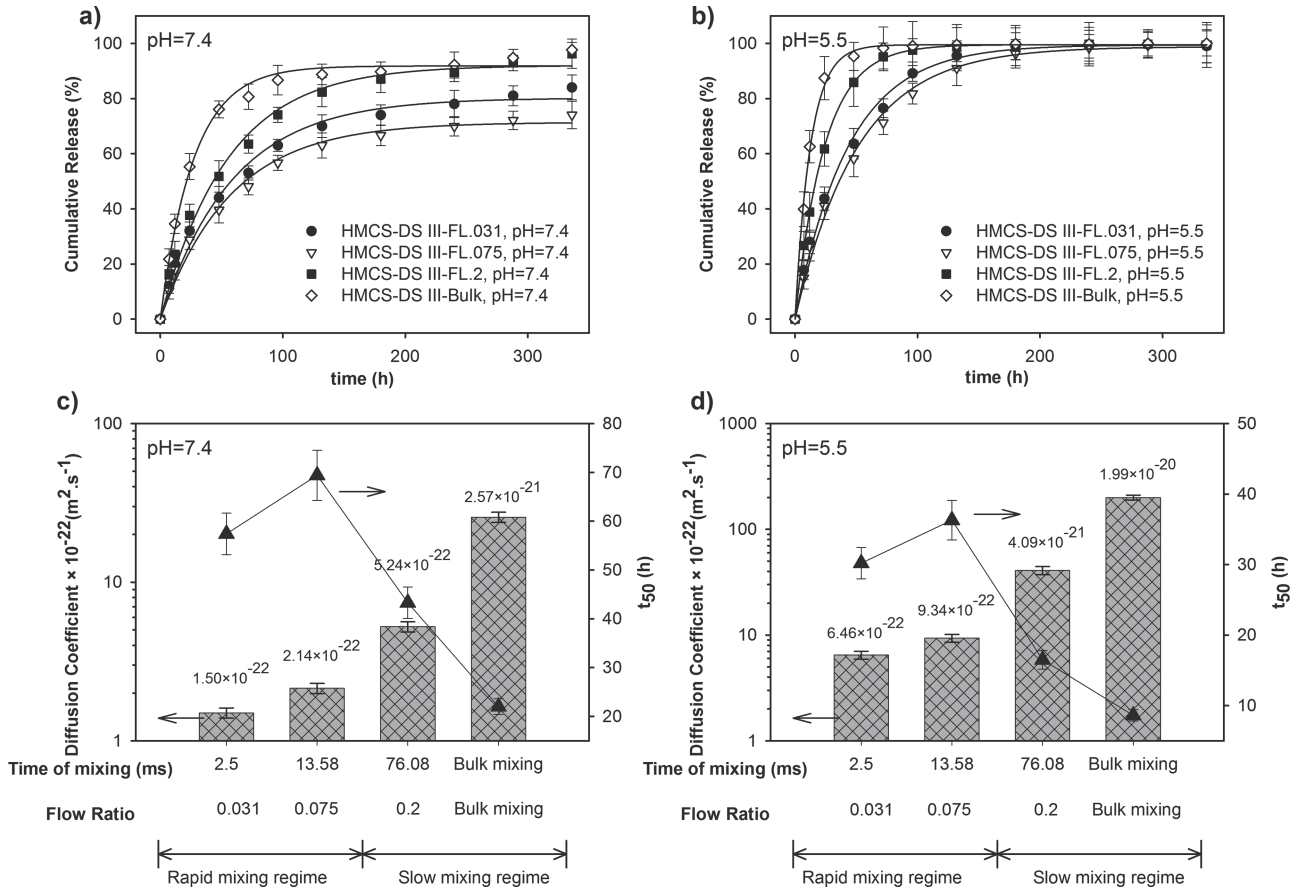

Figure 5. Cumulative in vitro release of PTX from HMCS DS III nanoparticles at 37 °C and (a) pH 7.4 and (b) pH 5.5 (Mean ± SD, n = 4 independent experiments.) Data are fitted with Equation (2) (R^2 0.98). Calculated diffusion coefficients at 37 °C of PTX within nanoparticles at (c) pH = 7.4 and (d) pH = 5.5, and relevant time for releasing 50% of the loaded drug.

the radius of the nanoparticles (based on DLS results). The calculated values for the diffusion coefficient, and the time needed for 50% of drug release (t_{50}), are shown in Figure 5c,d. As can be seen, microfluidic nanoparticles have considerably lower diffusion coefficients along with extended t_{50}, which is highly desirable for controlled release applications. These results are consistent with the more compact nanostructures of the nanoparticles formed in the rapid mixing regime (Figure 1b). Therefore, these results agree in signifying the important role that assembly time plays in the loading and release behavior of the nanoparticles.

Although PTX encapsulation efficiency inside nanoparticles can be tuned through our microfluidic platform, additional information is needed about the functionality of the encapsulated PTX. To verify the continued potency of nanoparticle loaded PTX, their response during storage was measured (**Figure 6**a,b). At both 25 °C and 37 °C, PTX activity decreased over time, but the half-life (50% of normalized activity) of PTX encapsulated by bulk mixing was more than an order of magnitude longer than free PTX, and PTX encapsulated with microfluidic assembly remained above the 50% activity threshold throughout the entire experiment (Figure 6). Such a prolonged thermal stability can elongate the effective circulation time of PTX in the human body. This is likely due to the hydrophobic protection of HMCS carbohydrate moieties inside the self-assembled nanoparticles, which protects the PTX from direct water molecule contact. Microfluidically synthesized nanoparticles better protected their cargo at both tested temperatures.

To evaluate the pH-dependent PTX release of the nanoparticles, and as an in vitro simulation of circulating nanoparticles encountering a tumor, we examined their release profile after changing the pH from 7.4 to 6.5, which mimics the acidic extracellular pH of tumors.[27] We also reduced the pH to 5.5, mimicking the intracellular (lysosomal) environment. Before starting the release experiments, the NPs were kept in PBS for 72 h to remove any adsorbed PTX, and to advance past their initial high release rate period. As shown in **Figure 7**, microfluidically prepared nanoparticles can maintain their loaded drug in physiological pH and during blood circulation. These nanoparticles are designed to accumulate in tumor regions due to the enhanced permeability and retention effect, and after entering into a tumor region (pH 6.5) they will start to release their anticancer drug faster. Particles also respond to the further change in pH when the pH is reduced to 5.5, an indication of cellular uptake.

As previously discussed, due to their surface potential, these NPs are rapidly endocytosed by cancer cells (e.g. breast cancer

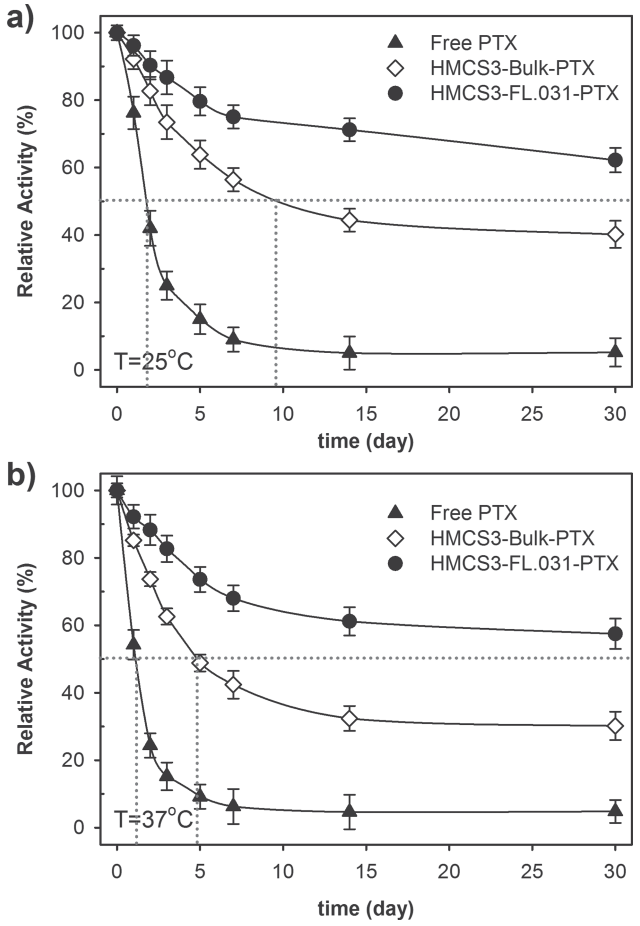

Figure 6. Relative activity of PTX at (a) 25 °C and (b) 37 °C for free PTX and PTX loaded HMCS nanoparticles.

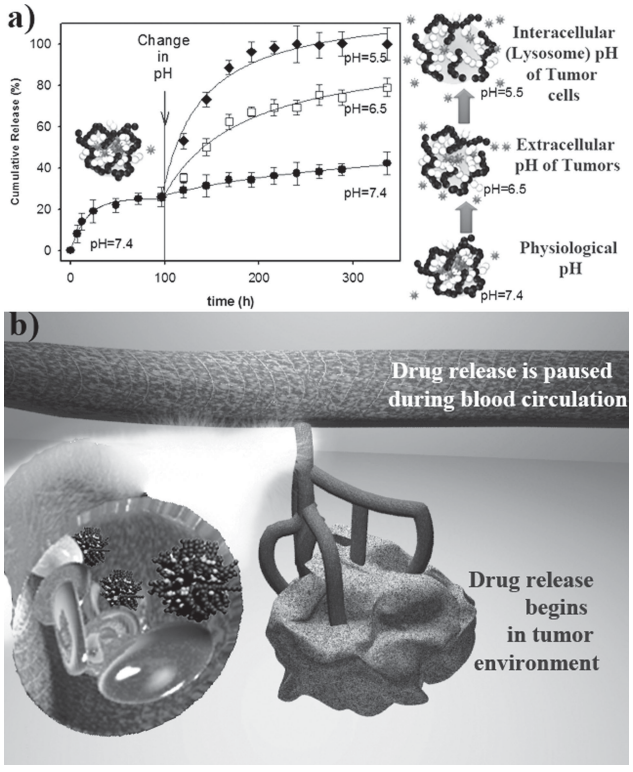

Figure 7. Controlled release of PTX from microfluidically synthesized nanoparticles (FL = 0.031) after media pH change, at 37 °C (Mean ± SD, n = 4 independent experiments.).

MCF-7 cells). All these positively charged NP attributes combine to offer a synergetic effect in potential cancer treatment. One important expectation for a good cancer therapy delivery vehicle is to maximize the lethal effects of the drug in the tumor cells proximity. Empty nanoparticles synthesized through both microfluidics and bulk mixing are not toxic, even at high concentrations (**Figure 8**). However, free PTX is toxic, and the half-maximal inhibitory concentration (IC_{50}) for MCF-7 cells is about 1 nM. PTX toxicity is significantly enhanced through encapsulation in HMCS nanoparticles. This phenomenon is likely due to the small size of the particles which are endocytosed into the cells (Figure 3), where they release their drugs into the cytosol, which greatly increases the drug's effectiveness.

These results demonstrate our ability to increase non-specific nanoparticle uptake and drug delivery, in vitro, by only modifying the nanoparticle structure. Other design considerations for *in vivo* applications, such as renal clearance, the blood brain barrier, and specific cell type targeting, will need to be optimized in future work. A key advantage of nanoparticle drug delivery is the ability to separately control and adjust the drug cargo type, the delivery mechanism, and the targeting functionality. This strength is also a weakness, however, as optimizing nanoparticle properties may require the addition of stealth or targeting coatings and different cargo or carrier materials, often with seemingly conflicting design requirements. The uncertainty of future demands across such a large parameter space necessitates an adjustable fabrication platform that maximizes nanoparticle flexibility, which we think microfluidic assembly can provide.

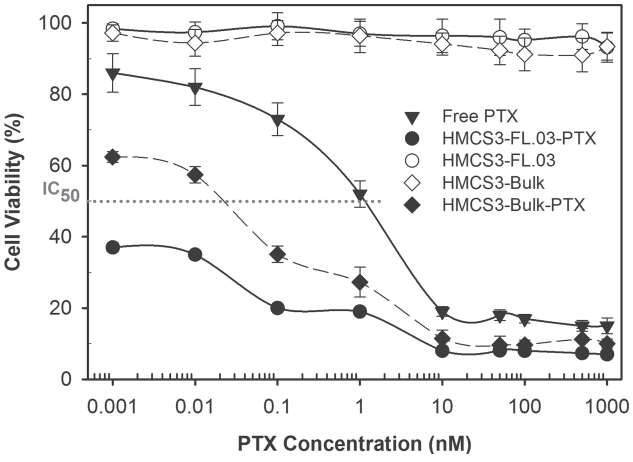

Figure 8. MTT based cell viability assay of MCF-7 cells after 72 h of exposure to free PTX, PTX loaded nanoparticles, and unloaded nanoparticles at 37 °C. Unloaded nanoparticles were used as a negative control to the PTX loaded NPs, and are plotted on the abscissa so that the number of nanoparticles in corresponding trials is the same.

3. Conclusions

Here we described the fine-tuning of hydrophobically-modified chitosan nanoparticles using a T-shaped PDMS microfluidic device. With this increased control over nanoparticle self-assembly, we can regulate the final nanoparticle size, compactness, surface charge, drug loading efficiency, and release rate, all important properties for nanoparticle drug delivery systems. Nanoparticle assembly is driven by controlled pH changes in a water environment; no organic solvents are used. These nanoparticles can encapsulate hydrophobic anti-cancer drugs, like paclitaxel, at efficiencies above 95%, and preserve the drug's potency better than conventional encapsulation methods. Nanoparticle uptake was also enhanced by tuning the nanoparticle size and surface charge, which dramatically increased the drug's potency. These microfluidic synthesized nanoparticles, due to their compact nanostructures, have a low release rate at pH 7.4, which is desirable for long-term circulation stability. However, when these particles are exposed to pH 5.5, common in tumors, the nanoparticles release their contents over an order of magnitude faster. In sum, we have developed a system to tune the properties of nanoparticle drug delivery systems in a way that maximizes their effectiveness across the relevant parameter space, and more generally, this microfluidic system has applications beyond drug delivery, as the ability to carefully control self-assembly conditions has implications throughout the field of materials science.

4. Experimental Section

Hydrophobic modification of chitosan was performed according to reported protocols.[8,9] Briefly, one gram chitosan (CS; medium molecular weight, 280–000 g/mol, degree of deacetylation 83%, Fluka) was stirred for 12 h in aqueous acetic acid (50 mL, 1% w/v; Sigma-Aldrich). Once dissolved, the solution was filtered with a 0.45 µm Nylon syringe filter. The pH was then adjusted to 5.5 by addition of sodium hydroxide (Sigma-Aldrich). A solution of 300 mg palmitic acid N-hydroxysuccinimide ester (Sigma–Aldrich) in absolute ethanol (Sigma-Aldrich) was added drop-wise to the chitosan solution at 98 °C under reflux and reacted for 48 h. The solution was then cooled down to room temperature and, after adding acetone, was precipitated by adjusting the solution pH to 9.0. The precipitated polymer was then filtered twice, washed with an excess of acetone, and vacuum-dried at room temperature. The prepared hydrophobically modified chitosan (HMCS) was analyzed by ^{1}H NMR (Bruker 400 MHz).

The degree of substitution (DS) of palmitoyl groups on chitosan was determined using the ninhydrin assay.[8] HMCS was dissolved in an aqueous acetic acid and then 0.5 mL of 4M acetic acid/acetate buffer (pH= 5.5) was added into 0.5 mL of the prepared solution. 1 mL of ninhydrin reagent (Sigma–Aldrich) was then added and test tubes were placed in a boiling water bath for 20 min. The solutions were then cooled and their absorbances at 570 nm were read. The unmodified chitosan solution was used as a control and the acetic acid/acetate buffer was used as a blank.[18]

Fluorescein-modified hydrophobically modified chitosan (f-HMCS) were synthesized based on the reaction between fluorescein isothiocyanate (FITC) and the chitosan as described in the literature.[34] Briefly, prepared FITC in methanol (2 mg mL^{-1}) was added gradually to the solution of HMCS in 1% w/v of acetic acid. After 5 h of reaction in a dark environment, at ambient temperature, the FITC-labeled chitosan was precipitated in 0.2 M NaOH and separated from unreacted FITC in a Sephadex G-50 column with 1/15 M phosphate buffer/0.2 M NaCl as an elution solvent. Fractions containing the labeled polymer were collected and dialyzed using a 3 kDa molecular weight cut-off dialysis cartridge (Thermo Scientific, Rockford, IL) against deionized water until no fluorescence was detected in the supernatant (about 4 days) before freeze drying. The resultant f-HMCS was used to prepare the fluorescent labeled NPs as described above.

Microfluidic Fabrication: Microfluidic devices were fabricated with poly(dimethylsiloxane) (PDMS) using a standard micromolding process. To make the master molds, silicon wafers were spincoated with SU-8 50 photocurable epoxy to a thickness of 60 µm. Baking, lithography, and development procedures were performed at the EPFL Center for Micronanotechnology (CMi) to obtain negative microchannels on the wafer. The wafers were then annealed at 150 ºC to eliminate surface cracks in the SU-8. After annealing, the surface of the resultant molds was coated with a self-assembled monolayer of trimethylethoxy silane by vapor exposure for 40 min. The SAM prevents PDMS from sticking to the mold. PDMS (Sylgrad 184) monomer and curing agent were mixed in a weight ratio of 10:1, pored over the mold, degassed in desiccators and cured in an oven at 80 ºC for 1 h. After curing, the PDMS was removed from the mold and in-/outlet holes were punched using a 150 µm diameter punch. The PDMS was then bonded to a glass slide using oxygen plasma (100 mW, 1 min). The PDMS microfluidic device had two inlets for water with a pH of 9, one for the aqueous solution of HMCS with the pH of 5.5, and one outlet (Scheme 1). The water stream was split into two, in order to achieve two water streams at the flow focusing T-junction. The mixing channel was 150 µm wide, 60 µm high and 1 cm long.

For bulk synthesis of HMCS based nanoparticles, polymeric solutions were prepared by dissolving 2.5 mg mL^{-1} HMCS in 1% w/v acetic acid solution under constant stirring. The nanoprecipitation of HMCS molecules and formation of the nanoparticles were performed by drop-wise addition of 1M NaOH to adjust the pH to 7.4.

For drug loaded nanoparticles, Paclitaxel (Sigma-Aldrich) was dissolved in acidic water (pH 4.5) and mixed with the polymeric solution. The preparation of nanoparticles is detailed above.

Atomic force microscopy (AFM; Bruker's Dimension FastScan), and transmission electron microscopy (TEM; CM200-FEG-Philips) were used to characterize morphology of the HMCS nanoparticles. A dilute suspension of nanoparticles was prepared and deposited onto a Cu TEM grid with a carbon film. The shape and size of the particles was characterized via diffraction (amplitude) contrast and, for crystalline materials, through high resolution (phase contrast) imaging. The TEM used a LaB6 source operating at 100 kV. The images were characterized using ImageJ software with at least 20 different measurements.

Dynamic light scattering (DLS) as well as zeta potential measurements were performed using a Zetasizer (Zetasizer 3000HS, Malvern Instruments Ltd., Worcestershire, UK) in backscattering mode at 173° for water diluted systems.

Transmittance of the prepared samples was measured at room temperature (20 °C) with a Shimadzu UV mini 1240 UV/visible spectrophotometer with a wavelength of 550 nm. Turbidity (τ) was calculated from the transmittance using Lambert-Beer's law:[23,24]

$$\tau = -\frac{1}{L} ln \left(\frac{I_t}{I_0}\right) \quad (3)$$

where L is the length of light path in the sample cell (1.0 cm quartz cuvette), I_t is the intensity of the light transmitted through the sample, and I_0 is the intensity of the light transmitted through the solvent (deionized water). Each measurement was performed at least three times, and the mean values are reported in Table S2.

To determine the in vitro drug release profile, lyophilized PTX-loaded nanoparticles (1 mg) were dispersed in 1 mL of phosphate buffered saline (1X PBS, pH 7.4). The solutions were placed into a 3 kDa molecular weight cut-off dialysis cartridge (Thermo Scientific, Rockford, IL). The cartridge was immersed in 1 L PBS and gently shaken in a 37 °C water bath. At predetermined intervals, buffered solution samples were collected and replaced with an equivalent volume of fresh PBS.

The PTX concentration was measured with reversed-phase high-performance liquid chromatography (HPLC) by mixing 1 mL of sample with 1 mL of acetonitrile as follows: A C18 column was used as the stationary phase, while the mobile phase consisted of acetonitrile:water (60:40 vol/vol). Separation was carried out at a flow rate of 1 mL min^{-1}. PTX was detected at a wavelength of 230 nm. This method was evaluated over a linear range of 1–100 μg mL^{-1}. In this range, the percent deviation from theoretical values was less than 5% and the R-square values remained less than 4% using clean PTX standards.

The PTX concentration in the solution was corrected for sampling effects according to:[35]

$$C_n^1 = C_n[V_T/(V_T - V_S)](C_{n-1}^1/C_{n-1}), \quad (4)$$

where C_n^1 is the corrected concentration of the nth sample, C_n is the measured concentration of PTX in the nth sample, C_{n-1} the measured concentration of the (n–1)th sample, V_T is the volume of the receiver fluid and V_S represents the volume of the drawn sample (1 mL).

Encapsulation efficiency of the nanoparticles and loading efficiencies were determined by applying the following equations:

$$\text{PTX Loading content} = (\text{Weight of the loaded PTX} / \text{Weight of the nanoparticle}) \times 100 \quad (5)$$

$$\text{PTX Loading efficiency} = (\text{The amount of PTX in the nanoparticles} / \text{initial amount of the PTX in nanoparticles}) \times 100 \quad (6)$$

Relative activities of PTX were estimated by calculating the maximum rate of tubulin polymerization relative to the standard samples. Stability of the free and encapsulated PTX inside different types of nanoparticles was evaluated by measuring the variations of their activities using the tubulin protein assay after storage at 25 °C and 37 °C for 1–14 days in a 96-well microtiter plates according to previously established protocols.[36,37] Briefly, at defined time intervals nanoparticles were separated using centrifugation and redispersed in water at pH 4.5 to extract the PTX from the nanoparticles. The PTX was then separated using HPLC to perform a tubulin protein assay. PTX at defined concentrations was reacted with tubulin protein solution (general tubulin buffer, tubulin glycerol buffer, 1 mM GTP) and the reaction was followed by measuring the increase in apparent absorption at 350 nm over 1 h at 37 °C using an ELISA plate reader (Safire II, Tecan Sales Switzerland AG, Mannedorf, CH).

The cellular uptake of FITC-labeled HMCS nanoparticles (f-HMCS NPs) were measured using flow cytometry, on a CyAn ADP Analyzer (FACS, Beckman Coulter, Inc). For the FACS analysis, Human breast adenocarcinoma (MCF-7) cells (10^6 cells) were dispersed into Eppendorf tubes. Then f-HMCS NPs were added at different concentrations of 50, 100, 200, and 400 μg mL^{-1}, except for the unstained negative control, and the cells were incubated for 2 h in normal medium in a tissue culture incubator. The cells were then washed using ice-cold PBS containing 10% FBS, and transferred into FACS tubes. All samples were kept on ice until FACS analysis.

MCF-7 cells were also used for cytotoxicity experiments. In vitro cytotoxicity assays were performed using HMCS NPs. MCF-7 cells cultured in DMEM medium (Sigma) without phenol red and supplemented with 10 % FBS. The cell cultures were cultured at 37 °C in a 5% CO_2 incubator.

The cytotoxicity tests were assessed using an MTT colorimetric assay.[38] Cytotoxicity of the nanoparticles was determined after 72 h incubation with MCF-7 cells.[39] To determine cell cytotoxicity/viability, the cells were plated at a density of 10 000 cells per well in 96 well plates and then incubated overnight. For paclitaxel treatment, a stock solution of paclitaxel (10 mg mL^{-1} in DMSO) was diluted to the defined concentration in culture medium. After treating the samples for 72 h, the MTT solution (20 μL, 5 mg mL^{-1} in phosphate buffer pH 7.4) was added, and the cells were incubated for 2 h. The absorbance of the reduced MTT (formazan) solubilized in DMSO was then measured using a plate reader (Safire II, Tecan Sales Switzerland AG, Mannedorf, CH) at 570 nm.

The control experimental medium contained no nanoparticles. The samples were maintained with uniform drug concentration. The spectrophotometer was calibrated to zero absorbance using culture medium without cells. The relative cell viability (%) related to the control wells, containing cell culture medium without nanoparticles, was calculated by $[A]_{test}/[A]_{control} \times 100$, where $[A]_{test}$ is the absorbance of the test sample and $[A]_{control}$ is the absorbance of the control sample.

All the experiments were conducted at least in triplicate. The statistical analysis of the experimental data is done using the Student's t-test, and the results are presented as mean ±S.D. Statistical significance was accepted at a level of $p < 0.05$.

Supporting Information

Supporting Information is available from the Wiley Online Library or from the author.

Acknowledgements

Authors would like to thank Prof. Karl I. Jacob from Georgia Institute of Technology, Atlanta, Dr. H. Van Lintel and Mr. M. Taghipoor in the LMIS4-EPFL for their helpful technical assistance and from Dr. Carrie E. Brubaker (EPFL-IBI-LMRP), Prof. Jeffrey A. Hubbell (EPFL-IBI-LMRP) and Prof. Francesco Stellacci (EPFL-STI-IMX-SunMIL) for their helpful discussions and critical reading of the manuscript. This research is performed in the framework of Biologically Inspired Developing Advanced Research (BiDAR) group.

Received: May 12, 2013
Revised: June 3, 2013
Published online: August 5, 2013

[1] D. Hanahan, Robert A. Weinberg, *Cell* **2011**, *144*, 646.
[2] D. A. LaVan, T. McGuire, R. Langer, *Nat. Biotechnol.* **2003**, *21*, 1184.
[3] J. A. Hubbell, A. Chilkoti, *Science* **2012**, *337*, 303.
[4] A. Schroeder, D. A. Heller, M. M. Winslow, J. E. Dahlman, G. W. Pratt, R. Langer, T. Jacks, D. G. Anderson, *Nat. Rev. Cancer* **2012**, *12*, 39.
[5] W. B. Liechty, N. A. Peppas, *Eur. J. Pharm.Biopharm.* **2012**, *80*, 241.
[6] S. E. A. Gratton, P. A. Ropp, P. D. Pohlhaus, J. C. Luft, V. J. Madden, M. E. Napier, J. M. DeSimone, *Proc. Natl. Acad. Sci. USA* **2008**, *105*, 11613.
[7] N. Kamaly, Z. Xiao, P. M. Valencia, A. F. Radovic-Moreno, O. C. Farokhzad, *Chem. Soc. Rev.* **2012**, *41*, 2971.
[8] Y.-L. Chiu, Y.-C. Ho, Y.-M. Chen, S.-F. Peng, C.-J. Ke, K.-J. Chen, F.-L. Mi, H.-W. Sung, *J. Controlled Release* **2010**, *146*, 152.
[9] Y.-L. Chiu, S.-C. Chen, C.-J. Su, C.-W. Hsiao, Y.-M. Chen, H.-L. Chen, H.-W. Sung, *Biomaterials* **2009**, *30*, 4877.
[10] F. S. Majedi, M. M. Hasani-Sadrabadi, S. Hojjati Emami, M. A. Shokrgozar, J. J. VanDersarl, E. Dashtimoghadam, A. Bertsch, P. Renaud, *Lab Chip* **2013**, *13*, 204.
[11] F. Schmitt, L. Lagopoulos, P. Käuper, N. Rossi, N. Busso, J. Barge, G. Wagnières, C. Laue, C. Wandrey, L. Juillerat-Jeanneret, *J. Controlled Release* **2010**, *144*, 242.

[12] M. Hamidi, A. Azadi, P. Rafiei, *Adv. Drug Deliv. Rev.* **2008**, *60*, 1638.
[13] M. M. Hasani-Sadrabadi, F. S. Majedi, J. J. VanDersarl, E. Dashtimoghadam, S. R. Ghaffarian, A. Bertsch, H. Moaddel, P. Renaud, *J. Am. Chem. Soc.* **2012**, *134*, 18904.
[14] Y. Kim, B. Lee Chung, M. Ma, W. J. M. Mulder, Z. A. Fayad, O. C. Farokhzad, R. Langer, *Nano Lett.* **2012**, *12*, 3587.
[15] R. Karnik, F. Gu, P. Basto, C. Cannizzaro, L. Dean, W. Kyei-Manu, R. Langer, O. C. Farokhzad, *Nano Lett.* **2008**, *8*, 2906.
[16] A.-L. Kjøniksen, C. Iversen, B. Nyström, T. Nakken, O. Palmgren, *Macromolecules* **1998**, *31*, 8142.
[17] E. Curotto, F. Aros, *Anal. Biochem.* **1993**, *211*, 240.
[18] S. Prochazkova, K. M. Vårum, K. Ostgaard, *Carbohydr. Polym.* **1999**, *38*, 115.
[19] F. S. Majedi, M. M. Hasani-Sadrabadi, S. H. Emami, M. Taghipoor, E. Dashtimoghadam, A. Bertsch, H. Moaddel, P. Renaud, *Chem. Commun.* **2012**, *48*, 7744.
[20] B. K. Johnson, R. K. Prud'homme, *Phys. Rev. Lett.* **2003**, *91*, 118302.
[21] C.-W. Wang, D. Sinton, M. G. Moffitt, *J. Am. Chem. Soc.* **2011**, *133*, 18853.
[22] P. M. Valencia, O. C. Farokhzad, R. Karnik, R. Langer, *Nat. Nanotechnol.* **2012**, *7*, 623.
[23] H. Jonassen, A.-L. Kjøniksen, M. Hiorth, *Colloid Polym. Sci.* **2012**, *290*, 919.
[24] H. Jonassen, A.-L. Kjøniksen, *Phys. Rev. E: Stat. Phys., Plasmas, Fluids, Relat. Interdiscip. Top.* **2011**, *84*, 022401.
[25] A. E. Nel, L. Madler, D. Velegol, T. Xia, E. M. V. Hoek, P. Somasundaran, F. Klaessig, V. Castranova, M. Thompson, *Nat. Mater.* **2009**, *8*, 543.
[26] T.-G. Iversen, T. Skotland, K. Sandvig, *Nano Today* **2011**, *6*, 176.
[27] K. Na, E. Seong Lee, Y. H. Bae, *J. Controlled Release* **2003**, *87*, 3.
[28] S. Mitragotri, J. Lahann, *Nat. Mater.* **2009**, *8*, 15.
[29] A. E. de Salamanca, Y. Diebold, M. Calonge, C. García-Vazquez, S. Callejo, A. Vila, M. J. Alonso, *Invest. Ophthalmol. Visual Sci.* **2006**, *47*, 1416.
[30] Z. Garaiova, S. P. Strand, N. K. Reitan, S. Lélu, S.Ø. Størset, K. Berg, J. Malmo, O. Folasire, A. Bjørkøy, C. de L. Davies, *Int. J. Biol. Macromol.* **2012**, *51*, 1043.
[31] J. Tian, V. J. Stella, *J. Pharm. Sci.* **2008**, *97*, 1224.
[32] Y. Fan, C. Li, H. Cao, F. Li, D. Chen, *Biomaterials* **2012**, *33*, 4220.
[33] M. S. Romero-Cano, B. Vincent, *J. Controlled Release* **2002**, *82*, 127.
[34] M. Huang, Z. Ma, E. Khor, L.-Y. Lim, *Pharm. Res.* **2002**, *19*, 1488.
[35] S. H. Emami, Z. H. Pirbasti, M. M. Hasani-Sadrabadi, S. S. Kordestani, *J. Appl. Polym. Sci.* **2011**, *122*, 3048.
[36] M.-Y. Hua, H.-W. Yang, C.-K. Chuang, R.-Y. Tsai, W.-J. Chen, K.-L. Chuang, Y.-H. Chang, H.-C. Chuang, S.-T. Pang, *Biomaterials* **2010**, *31*, 7355.
[37] S. Sharma, T. Ganesh, D. G. I. Kingston, S. Bane, *Anal. Biochem.* **2007**, *360*, 56.
[38] G. Ciapetti, E. Cenni, L. Pratelli, A. Pizzoferrato, *Biomaterials* **1993**, *14*, 359.
[39] Y. Lee, R. Graeser, F. Kratz, K. E. Geckeler, *Adv. Funct. Mater.* **2011**, *21*, 4211.